JOURNAL OF SPACECRAFT AND ROCKETS
Vol. 42, No. 3, May–June 2005

Application of Accelerometer Data to Mars Odyssey Aerobraking and Atmospheric Modeling

R. H. Tolson*
North Carolina State University, Hampton, Virginia 23666
A. M. Dwyer† and J. L. Hanna†
NASA Langley Research Center, Hampton, Virginia 23681
G. M. Keating‡
George Washington University, Newport News, Virginia 23606
and
B. E. George,§ P. E. Escalera,§ and M. R. Werner§
George Washington University, Hampton, Virginia 23681

Aerobraking was an enabling technology for the Mars Odyssey mission, even though it involved risk due primarily to the variability of the Mars upper atmosphere. To reduce the risk, numerous analyses, based on various data types, were performed during operations. The use of one such data type, measurements from spacecrafts accelerometers, for determining atmospheric density during Odyssey aerobraking operations is reported. Accelerometer data were analyzed in near real time to provide estimates of density at periapsis, maximum density, density scale height, latitudinal gradient, longitudinal wave variations, and location of the polar vortex. Summaries of the aerobraking phase of the mission, the accelerometer data analysis methods and operational procedures, applications to determining thermospheric properties, and several remaining issues on interpretation of the data are discussed. Although acceleration was measured along three orthogonal axes, only data from the component along the axis nominally into the flow were used during operations. For a 1-s count time, the rms noise level, derived from the acceleration, varied from 0.07 to 0.5 mm/s^2, permitting density recovery to between 0.15 and 1.1 kg/km^3, or about 2% of the mean density at periapsis during aerobraking. Preflight estimates of natural variability based on Mars Global Surveyor accelerometer measurements proved reliable in the midlatitudes but overestimated the variability inside the polar vortex.

Nomenclature

A	=	reference area for aerodynamics, m^2
$\boldsymbol{a}$	=	acceleration, m/s^2
C_y	=	aerodynamic force coefficient along body y axis
H_s	=	density scale height, km
h	=	areodetic altitude, km
h_0	=	areodetic reference altitude, km
J_2	=	second zonal harmonic gravity potential coefficient
J_3	=	third zonal harmonic gravity potential coefficient
L_s	=	celestial longitude of Mars measured from the Mars vernal equinox, deg
m	=	Odyssey mass, kg
Nq	=	Nyquist, samples/s
q	=	dynamic pressure, N/m^2
$\boldsymbol{r}$	=	position of accelerometer in body system relative wind unit vector $\boldsymbol{m}$, origin is center of mass
u_x	=	x-axis component of relative wind unit vector
u_z	=	z-axis component of relative wind unit vector
V	=	spacecraft speed relative to atmosphere, m/s
ΔV	=	change in velocity with time, m/s
ρ	=	density, kg/km^3
ω	=	body angular rate, deg/s

Received 30 December 2002; accepted for publication 4 November 2004.

*Professor, Department of Mechanical and Aerospace Engineering and Marine, Earth and Atmospheric Sciences, National Institute of Aerospace, 144 Research Drive. Associate Fellow AIAA.

†Aerospace Engineer, Mail Stop 489, Exploration Systems Engineering Branch. Member AIAA.

‡Senior Research Staff Scientist, Mechanical and Aerospace Engineering Department, 31 Cherbourg Drive. Associate Fellow AIAA.

§Graduate Research Scholar Assistant, Mechanical and Aerospace Engineering Department.

Introduction

AEROBRAKING is the utilization of atmospheric drag for beneficial orbit changes via multiple passes through an atmosphere. The first application of aerobraking in a planetary mission was during the Magellan mission at Venus.[1] To increase imaging radar and gravity field resolution in the polar region, aerobraking was performed during the extended mission in 1993 over about 750 orbital passes to reduce the eccentricity from 0.3 to 0.03 in about 70 days. During Magellan, adjustments were made to the Venus atmospheric model based on orbital decay drag data. The second application began in September 1997 when over 850 Mars Global Surveyor (MGS) aerobraking passes were used to reduce the post-Mars orbit insertion (MOI) period from about 45 h to about 2 h, saving an equivalent impulsive ΔV of approximately 1200 m/s (Ref. 2). MGS was the first planetary mission in which aerobraking was essential for mission success. Whereas the Venusian atmosphere demonstrated less than 10% 1-σ orbit-to-orbit variability in density, the Mars atmosphere demonstrated between 30 and 40%. During MGS, persistent density waves were found to exist in the equatorial region that could produce nearly a factor of two change in density from trough to peak. Furthermore, a regional dust storm in the southern hemisphere produced over a factor of two increase in density at the periapsis latitude of 60°N (Ref. 3).

The primary drag surfaces for Magellan, MGS, and Odyssey were the solar arrays. Solar array temperatures were the preaerobraking criteria limiting the pace of aerobraking. Because of a damaged solar array, MGS aerobraking was actually limited by maximum dynamic pressure during each pass at about one-half of the heating limit.[2] The large systematic atmospheric variations discovered

during MGS, and the random variations confirmed by MGS, were included in the Odyssey design. Nevertheless, the mission failures during the previous opportunity lead to numerous additional atmospheric modeling activities,[4] mission simulations,[5] and thermal analyses[6] before Odyssey MOI and during the aerobraking mission to determine thermospheric properties of the Mars atmosphere that are described herein.

Odyssey Aerobraking Mission Summary

A detailed overview of the aerobraking phase is given elsewhere,[7] and so only a summary is given here. The aerobraking configuration is shown in Fig. 1. Though not shown here, the bus is surrounded by thermal insulation. The configuration provides strong aerodynamic stability about the body z axis, which nominally points toward the center of Mars during aerobraking. The spacecraft is nearly neutrally stable about the y axis, which is along the velocity direction and normal to the plane of the solar array. The y axis is within 4 deg of the aerodynamic trim direction. The photovoltaic cells are oriented away from the flow to minimize cell heating.

After MOI on 24 October 2001, the orbital period was 18 h, and the goal of aerobraking was to reduce this period to 2 h by about 15 January 2002. The reference period decay profile, developed just after MOI, is shown in Fig. 2. Also shown is the actual orbital period achieved during aerobraking. The first few orbits were spent checking spacecraft systems before the periapsis altitude was dropped into the sensible atmosphere. The walk-in phase began with orbit 6 with a barely measurable atmospheric effect at 158-km altitude. Orbit 7 was the first aerobraking pass with a periapsis altitude of 136 km and a maximum density of about 1.5 kg/km^3. Orbits 17–19 began the main aerobraking phase with periapsis altitudes between 110.5 and 110.9 km and densities between 23 and 40 kg/km^3. The large variations in density predicted by the MGS experience were clearly present again. The actual orbital decay fell about 50 min behind the target at orbit 75. The decay was a result of periapsis precessing toward the north pole and passing through the high variability region of the polar vortex. While inside the vortex, the variability was substantially lower, and aerobraking could be performed more aggressively, so that by orbit 245 the actual decay was 13 min ahead of the plan. After 77 days, aerobraking ended on 11 January 2002, 13 days earlier than the planned 90 days.

Orbital characteristics of interest for aerobraking are shown in Fig. 3 for the entire aerobraking phase. Figure 3 presents areodetic

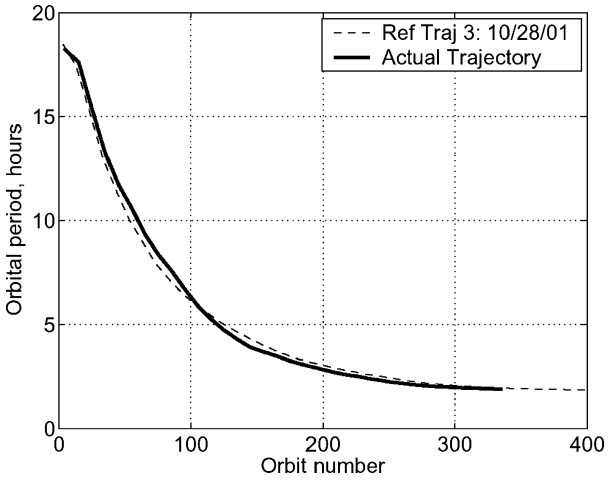

Fig. 2 Planned and actual orbital period during aerobraking.

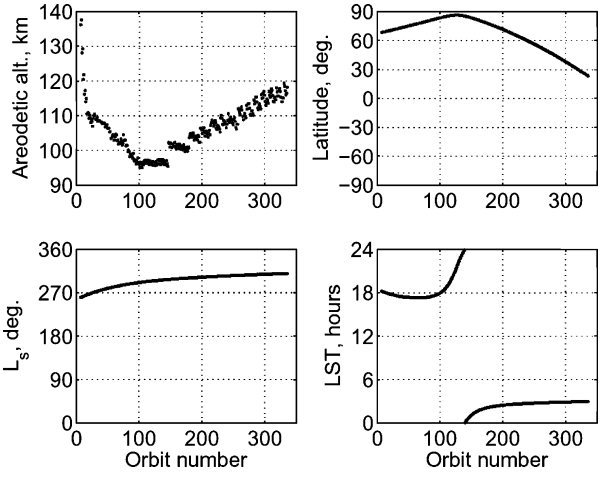

Fig. 3 Variables of interest for aerobraking for the Odyssey mission.

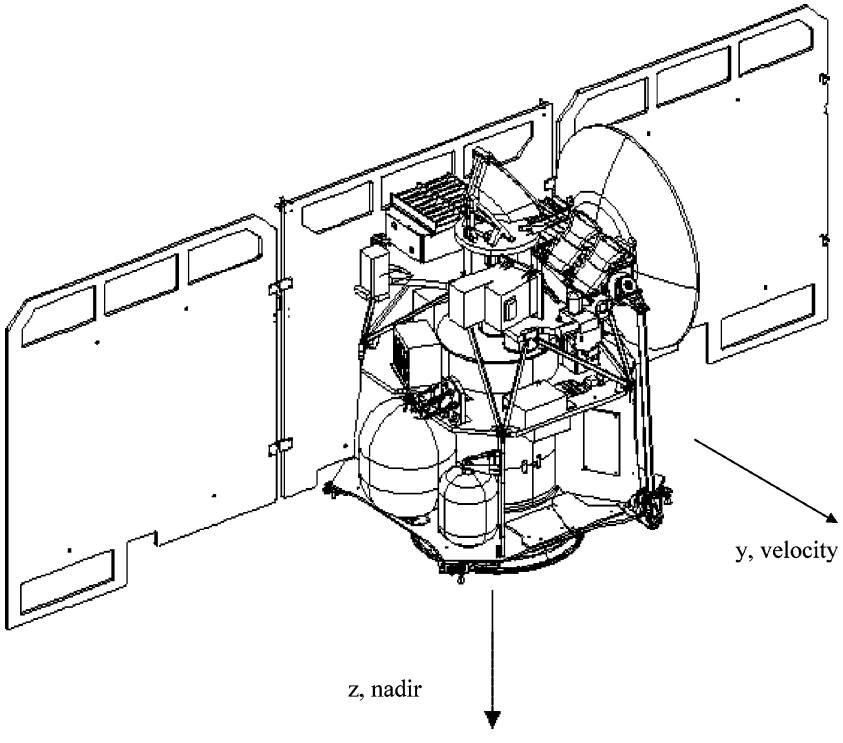

Fig. 1 Mars Odyssey spacecraft in aerobraking configuration, without thermal blankets.

altitude, latitude, local solar time, and L_s at periapsis. L_s is the celestial longitude of Mars measured from the Mars vernal equinox and is a measure of Mars season and distance from the sun. These four variables are thought to be the most significant in determining thermospheric mean properties. The altitude plot shows walk-in (orbits 6–16); main phase (orbits 17–248), where solar array temperature was the limiting factor; and walk-out (orbits 249–336), where orbital lifetime was the limiting factor. Precession of the line of apsides due to planetary oblateness J_2 moved periapsis poleward for the first 127 orbits and then toward the equator through the end of the mission. Orbit-to-orbit changes in periapsis altitude due to short period orbital perturbations are generally less than 1.5 km, and so changes larger than this value represent altitude adjustment maneuvers. Geodetic altitude is of interest because in a static atmosphere, equal pressure surfaces would be equipotential surfaces. Up to the time of maximum latitude, the J_3 long period variation in eccentricity causes periapsis altitude to increase with time. Likewise, as the orbit precesses northward due to J_2, the flattening of the planet causes areodetic altitude to increase. These two effects are the same order of magnitude and, when combined, result in a generally increasing periapsis altitude that provided a fail-safe situation early in the mission. Both effects reverse after the time of maximum periapsis altitude. It is clear that after orbit 140, these two effects continued to drive periapsis altitude lower into the atmosphere, requiring many maneuvers to keep the altitude in the aerobraking corridor. The general trends are primarily due to the latitudinal density gradient, which, at a constant areodetic altitude, causes density to decreases toward the colder pole. Local solar time (LST), as for all near-Hohmann transfers to outer planets, starts near 1800 (military clock) hrs. Because nodal regression is nearly zero for this nearly polar orbit, LST initially becomes smaller due to Mars orbital motion. Eventually, northward apsidal precession combined with Mars obliquity begins to dominate, and LST moves into night and rapidly shifts to morning hours as periapsis passes over the pole. The aerobraking mission lasted less than two Mars months, and so the season at Mars remained at northern hemisphere winter ($270 < L_s < 360$) throughout aerobraking.

Atmospheric Density Recovery

Because the y component of acceleration (Fig. 1) provides the largest signal-to-noise ratio, it was used to recover atmospheric density. The density recovery is based on Newton's second law and the definitions of aerodynamic coefficients,

$$ma_y = \rho V^2 C_y A/2 \tag{1}$$

Aerodynamic Database

To use acceleration measurements to determine atmospheric density from Eq. (1), an aerodynamic database of C_y is required that covers the spacecraft operational range. Main phase aerobraking was to take place at a nominal heat flux of about 0.3 W/cm^2, which corresponded to an atmospheric density of about 60 kg/km^3 and a Knudsen number of about 0.2, which is well into the transition region. The transitional region effects are included by making C_y a function of the density. Aerodynamic coefficients were generated for eight values of ρ up to at least twice the target density of 120 kg/km^3. Aerodynamic properties were calculated with direct simulation Monte Carlo (DSMC) and free-molecular flow codes.[8] The DSMC method was required to quantify aerothermodynamics accurately in the regions of highest dynamic pressure. Preflight attitude control simulations indicated that the relative wind could deviate as much as 20 deg from the y axis. DSMC and free-molecular simulations were performed over alpha and beta angle ranges up to 28.6 deg.

The force coefficient over the range of expected densities for flow along the y axis is shown in Fig. 4a. The value at $\rho = 0.001$ kg/km^3 is the free-molecular flow value used for lower densities. All calculations are based on assumed momentum accommodation coefficients of unity. The highest periapsis density encountered during aerobraking was on orbit 106 with a value of 107.4 kg/km^3. Contours of a typical C_y variation are shown in Fig. 4b for a density of 100 kg/km^3.

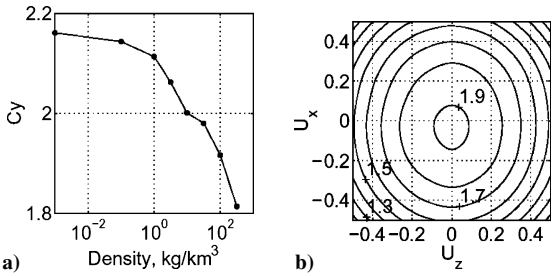

Fig. 4 Force coefficient of y axis over a range of atmospheric density for $u_x = u_z = 0$ and vs relative wind direction for $\rho = 100$ kg/km^3.

The variables $\boldsymbol{u}_x$ and $\boldsymbol{u}_z$ are the components of the relative wind unit vector in the spacecraft body coordinates shown in Fig. 1.

In the recovery of density from accelerometer data, the aerodynamic database is used in an iterative manner to solve Eq. (1). For each accelerometer measurement, the relative wind vector, assuming rigid rotation of the atmosphere with the planet, is determined from the attitude quaternions and the orbital ephemeris. Interpolation into the free-molecular versions of Fig. 4 is used to estimate C_y and then density. This density is used to update the C_y estimate, and the process continues until density converges to within 1%.

Accelerometer Data

Two inertial measurement units (IMU) are located on the upper deck of the spacecraft as shown in Fig. 1. The primary IMU was used throughout aerobraking. The internal orientation of two of the three accelerometers was not aligned with the body axes, and so data from these two accelerometers were combined in the ground data system (GDS) to form body axes accelerations. The principal acceleration used in the aerobraking analysis is the y direction. The accelerometers are located at $\boldsymbol{r} = (0.164, -0.544, \text{and } 1.137)$ m relative to the center of mass. The accelerometers and gyros were sampled at 200 Nq. The accelerometer data were quantized internally at 2.7 mm/s, but the least significant bit in the A/D converter was 0.0758 mm/s. For the purposes of density recovery, the high rate data were averaged over 1-s intervals. Up through orbit 136, all data recorded on the spacecraft at 200 Nq during an aerobraking pass were transmitted to the ground. However, as the eccentricity of the orbit decreased, the duration of the pass increased, and the full data set could not be recorded onboard. From orbit 137 to orbit 268, the first 50 samples were recorded for transmission and averaged each second. After orbit 268, only the first 20 samples, or 10% of the data, were transmitted each second. The measured acceleration is composed of a number of terms given by

$$\boldsymbol{a}_{\text{meas}} = \boldsymbol{a}_{\text{bias}} + \boldsymbol{a}_{\text{aero}} + \boldsymbol{a}_{\text{grav}} + \boldsymbol{a}_{ACS} + \boldsymbol{\omega} \times (\boldsymbol{\omega} \times \boldsymbol{r}) + \dot{\boldsymbol{\omega}} \times \boldsymbol{r} \tag{2}$$

where the terms are, respectively, acceleration due to the instrument bias, which was solved for aerodynamic forces used to determine density; gravity gradient (negligible); attitude control system (ACS) thruster activity; and angular motion of the accelerometer about the center of mass (two terms).

To illustrate the density recovery process, orbit 76 was selected. The orbit provides acceleration variations somewhat similar to the classic bell curve and also demonstrates some of the local variations during a pass. The telemetry accelerometer data along the y axis from which density was derived are shown in Fig. 5 for periapsis 76 (P076). Note that the onboard process for removing bias has left a small residual. The residual bias is removed as discussed hereafter, before density is derived from the data. Also, as described earlier, the process of deriving density from this acceleration involved an iterative scheme in which C_y is also recovered. The derived value of C_y for this pass is shown in the inset of Fig. 5. The C_y value decreases about 10% during the 150 s before periapsis, primarily due to the transition flow phenomena shown in Fig. 4. On the outbound portion of the pass, C_y returns to the free-molecular value just before 200 s and then decreases, as will be seen later, due to a change in heading that exposes less cross-sectional area to the flow.

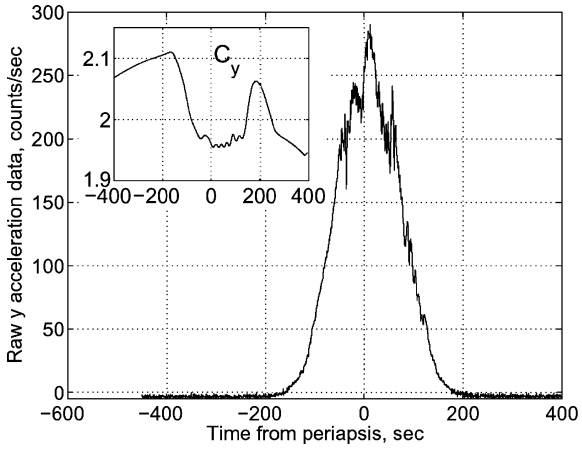

Fig. 5 Raw accelerometer counts and calculated axial aerodynamic force coefficient, P076.

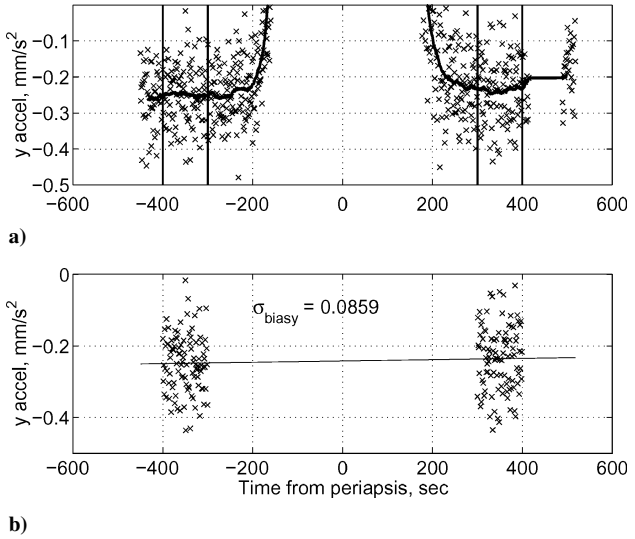

Fig. 6 Accelerometer bias removal process for P076.

Accelerometer bias was calibrated on the spacecraft by averaging measurements before encountering the atmosphere and after leaving the atmosphere. The bias, with an assumed constant value, was automatically subtracted from the measurements in the flight data system before the 1-s averaging was done. Subsequent analysis showed that the bias was different between the inbound and outbound legs of a pass, probably due to the general increase in temperature of the IMU throughout a pass. During the atmosphere modeling team (AMT) operations, a linear time-dependent bias was determined using inbound and outbound data. Through the pass, this model was evaluated at each observation time. An example of the process is shown in Fig. 6. Figure 6a shows the 1-s averaged acceleration data from the GDS. The line is the seven point running mean. To determine the bias, inbound and outbound data were selected visually, as indicated by the vertical lines and a least-square fit was used to obtain the linear model. The results are shown in Fig. 6b. The upward trend in bias of $\sim$0.01, though small compared to the rms residual of 0.086 mm/s, is clearly present, and the value is typical of most orbits. Note that the noise level of 0.086 mm/s is fairly close to the least significant bit value of 0.0758 mm/s. The noise level, determined during the bias calculation, for each orbit is shown in Fig. 7. The influence of changing the number of high rate samples from 200 to 50 and then to 20 is clearly evident. The lowest noise level corresponds to determining density to about 0.15 kg/km^3 and the largest level to about 1.1 kg/km^3.

Other Data Types

Angular motion contributions to the acceleration [Eq. (2)] were removed by using the rate gyro data that were received at 1 Nq. A

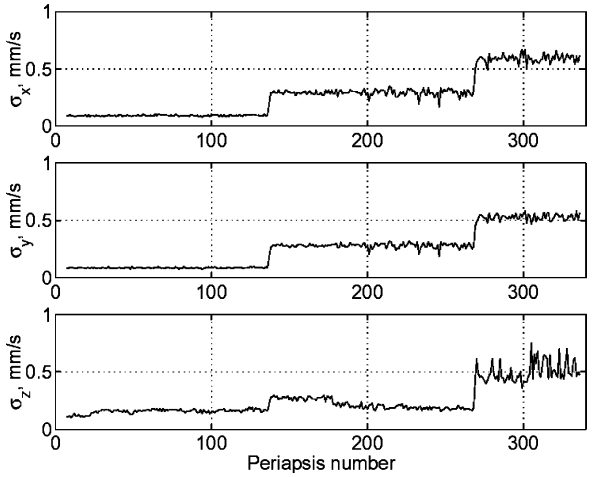

Fig. 7 Variation in accelerometer noise level throughout mission.

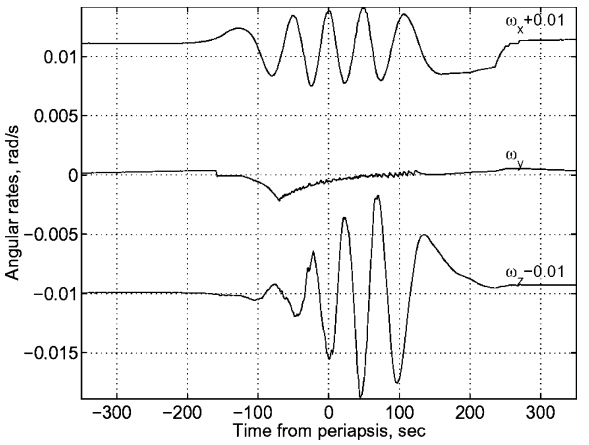

Fig. 8 Body angular rates during P076, rates displaced for clarity.

typical history of the body rates is shown in Fig. 8. Recall that rotations about the y axis (Fig. 1) have essentially no aerodynamic restoring force, but that motion about all three axes is coupled through the onboard momentum supplied by the reaction wheels. From the y axis angular rate data, it is seen that a thruster firing took place at about -150 s, followed by nearly continuous firings from -75 s through the rest of the pass, through about 120 s. These particular firings are coupled and theoretically produce no net acceleration of the spacecraft. The angular acceleration required in Eq. (2) was determined by fitting a polynomial to the rates and then differentiating the polynomial to determine the acceleration at the central point. For typical aerobraking passes, the maximum contribution due to these two terms is less than 0.5 mm/s^2, which, though small, is sufficiently large to require inclusion.

The orientation of the relative wind is obtained from the orbital ephemeris and the quaternions, also averaged to 1 Nq. The history of the relative wind is shown in Fig. 9 for orbit 76. The dashed line shows the relative wind before periapsis, whereas the solid line shows the relative wind after periapsis. From Figs. 9 and 8, note that aerodynamic torques are significant within about 150 s of periapsis; aerodynamic stability about the x and z axes is evident during these times. While in the atmosphere, deviations in u_x and u_z do not exceed 0.1, or less than 6 deg. The large outbound excursion is due to loss of aerodynamic stability on exiting the atmosphere, and so the spacecraft continues to rotate until the ACS becomes active. The excursion is the reason for the outbound decrease in C_y shown in Fig. 5. Note that the center of oscillation is near u_z of 0.07, corresponding to the equilibrium pitch angle of about 4 deg. This offset is primarily due to the geometric asymmetry caused by the high-gain antenna (Fig. 1).

Acceleration caused by thruster firing is the most difficult to remove. The factors that determine thruster effectiveness include

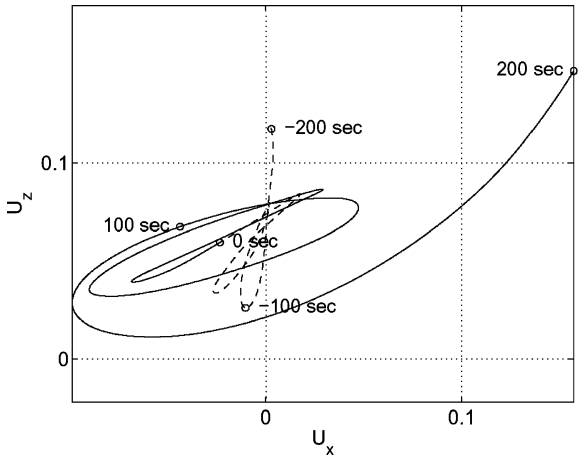

Fig. 9 Relative wind orientation during P076, times are seconds from periapsis.

specific impulse, propellant blowdown, temperature of the catalyst bed, and interference with the flow.[9] Past experience has shown that calibration within 50% is difficult for the short thrusting times and variable duty cycle typically associated with aerobraking attitude control.[10] The Odyssey thrusters were calibrated during interplanetary cruise,[11] but the calibration was found to be unreliable for the orbital phase. Because the contribution to the total acceleration is two orders of magnitude less than the periapsis drag effect, an ad hoc correction was made during each pass by the navigation team (NAV).[12] Because of the smallness of the correction, accelerometer data during operations were processed by the accelerometer team using the original interplanetary calibration. Postflight analysis of the data to extend the applicability to higher altitudes will require an improved calibration much like that performed for MGS data.[13]

Operational Procedures

There were three groups whose activities determined atmospheric models during operations. The Odyssey NAV, the atmospheric modeling team (AMT), and the atmospheric advisory group (AAG). The NAV utilized radio tracking data to determine the drag effect for each orbit.[7] The AMT utilized orbit determination products from NAV and accelerometer and other telemetry data to determine density every second throughout each aerobraking pass and to produce products for NAV, other NASA Langley Research Center (LaRC) teams,[6,9] and the AAG. AAG members were atmospheric scientists who reviewed and interpreted all available data and made recommendations to the project flight mission manager on periapsis altitude control maneuvers planned for the next maneuver opportunity.

Because there were no tracking data during the aerobraking phase of each orbit, radio tracking can essentially only determine the effective ΔV associated with the total drag pass. To map this into equivalent atmospheric parameters, the Mars Global Reference Atmospheric Model version 2000 (MarsGRAM),[14] was used as the underlying model for the time dependence of density during the pass, and NAV solved for a density multiplier that provided the best fit to pre- and postaerobraking tracking data for each orbit.[7] NAV utilized a density-dependent drag coefficient similar to that shown in Fig. 4, but neglected changes in drag due to spacecraft orientation shown in Fig. 4.

The operations plan called for NAV to process radio tracking data before the beginning of the drag pass and to provide predictions of the osculating elements at the subsequent periapses. These predictions were called preliminary orbits. A final orbit meant that both pre- and postaerobraking radio tracking data had been used in the orbit determination. Final orbit determinations were typically available from NAV about 2 h after periapsis. The AMT was located at NASA LaRC on the east coast, and operations typically began at 0700 hrs Eastern with transferring the previous day's data from the GDS to a NASA LaRC server. The AMT used final orbits, when available, to process accelerometer data accumulated overnight to determine periapsis density, maximum density, density scale height in the vicinity of periapsis, latitudinal gradient of both density and scale height, density and scale height at reference altitudes of 100, 110, . . . , 200 km, and other atmospheric variables. AMT also determined a MarsGRAM density multiplier directly from accelerometer data for comparison with the NAV value. These results were transmitted to a file server in flight operations for NAV and AAG review. At 1130 Pacific, the AAG met to discuss the results of the AMT and develop a maneuver recommendation and rationale. The maneuver options were no maneuver; up maneuver, that is, raise periapsis altitude by some number of kilometers; or down maneuver, that is, lower periapsis altitude by some number of kilometers. At 1430 Pacific, AAG, NAV, and Lockheed Martin Astronautics spacecraft system teams shared their recommendations with the flight mission manager for a final decision on the maneuver to be performed at the next opportunity.

Results

The first result developed by the AMT was the variation of density with time for each pass. These data were supplied to other teams to perform thermal analyses, flight dynamics simulations, and other studies. From the density vs time data, numerous parameters as just mentioned were extracted for AMT, AAG, and NAV use. Discussed hereafter are selected results on density vs time and density–altitude profiles both for one specific pass (P076) and later for additional representative profiles. Utilization of the orbit-to-orbit variations are then discussed in terms of prediction methods used for Odyssey. Finally, the method used to locate the polar vortex is presented.

P076 Density Profiles

Three realizations of density for P076 are shown in Fig. 10. The lower curve is the density at every second, the middle curve is the 7-point average, and the upper curve is the 39-point average. The curves are displaced for clarity. The seven-point averaging is done to remove local spatial variations in density but leaves mesoscale wave structure in the 100-km wavelength category. Some of these waves will be discussed later in the section on the polar vortex. The 39-point averaged data are used to estimate the mean atmosphere. The latter data were used to estimate density and density scale height at periapsis, latitudinal temperature and density gradients, and exospheric temperatures and to identify inbound and outbound properties for operational prediction.

The rapid changes in density at around −40 and +50 s are real variations in the atmosphere. Like these occurrences, it is not unusual for density to change by 30% in a few seconds. At 50 s from periapsis, the spacecraft downtrack speed is about 4.5 km/s, and the radial component is about 120 m/s. Figure 10 shows that the seven-point averaged profile suggest between three and five mesoscale waves about 20 s apart, or about 90 km if these are purely latitudinal structures.

To relate density vs time to atmospheric properties of interest to operations, a number of assumptions, simplifications, and

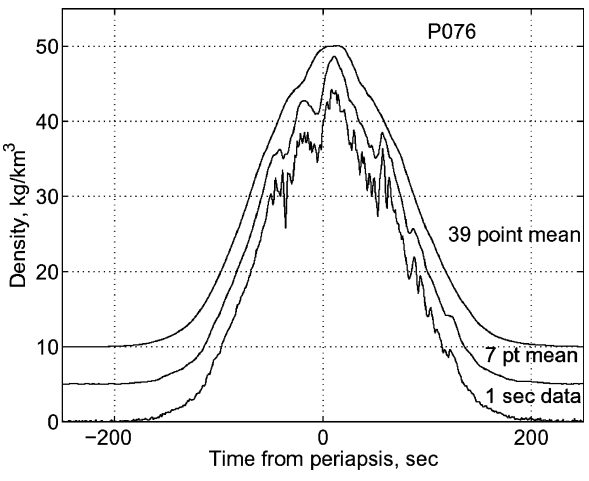

Fig. 10 Raw and smoothed derived density for P076.

considerations must be noted. First, Odyssey is in a near-polar orbit, and over a typical aerobraking pass the spacecraft is in the detectable atmosphere less than 400 s. While in the atmosphere, the latitude varies between ~20° at the beginning to ~50° at the end of the mission. The spacecraft travels between 12° and 26° in latitude while within one density scale height (~7 km) of periapsis. Thus, latitudinal variations cannot be ignored in the Odyssey profiles, and the common assumption of hydrostatic equilibrium is probably not applicable across an entire pass. With the 1-s data, density actually increases with altitude for many orbits; this pattern is common with the 7-s averaged data. Such variations suggest that the atmosphere is not in static equilibrium over even small scales.

The models most utilized during operations included the following: 1) the constant density scale height H_s model usually applied to a limited altitude range in the vicinity of a reference altitude h_0 on the inbound leg, the outbound leg, or near periapsis

$$\rho(h) = \rho(h_0)\exp[-(h - h_0)/H_s] \tag{3}$$

2) the model with constant density scale height but density at the reference altitude $\rho(h_0)$ varying linearly with latitude; and 3) the model with both reference altitude density and density scale height varying linearly with latitude. Under the assumptions of hydrostatic equilibrium and an isothermal atmosphere, density scale height is directly proportional to temperature. The last model is, thus, approximately equivalent to assuming that density and temperature at a reference altitude vary linearly with latitude. Deviation of the atmosphere from either hydrostatic equilibrium or constant temperature will bias temperature derived from the density scale height. Nevertheless, the few temperatures mentioned in this paper are derived under these assumptions.

The altitudinal profile for P076 is shown in Fig. 11. Within about 10 km of periapsis altitude, there is little difference between the density or density scale height for the inbound and outbound legs. Between 110- and 160-km altitude, the inbound leg, which is north of periapsis, appears to have a much lower temperature than the outbound leg. The difference is expected because the outbound leg is at a lower latitude and moving toward what should be the warmer equator. At 140 km, the local density scale heights are 6.40 km inbound and 8.84 km outbound. Interpreting these scale heights in terms of a locally isothermal atmosphere yields temperatures of 114 and 157 K, respectively.

The profile from MarsGRAM is also included in Fig. 11. MarsGRAM densities have been multiplied by 0.665 to provide the same effective total ΔV for the pass, that is, the same area under the density vs time curve. Near periapsis, the MarsGRAM model shows a much stronger latitudinal gradient than that inferred from the accelerometer data. The difference becomes larger with altitude with MarsGRAM predicting a factor of 3.5 density ratio between

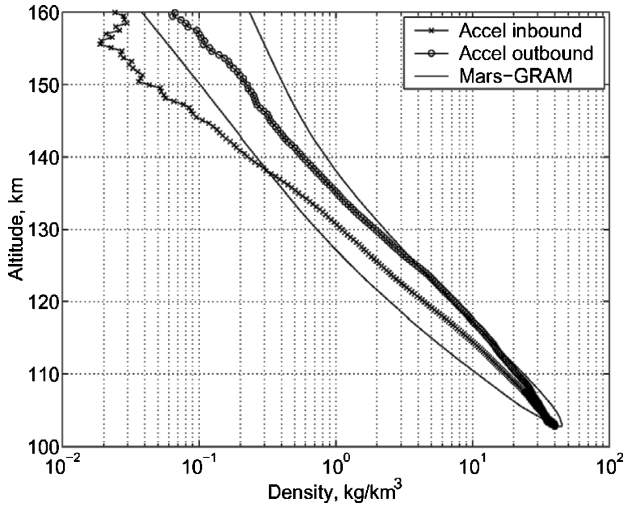

Fig. 11 Derived density vs altitude for P076 compared with scaled MarsGRAM profile.

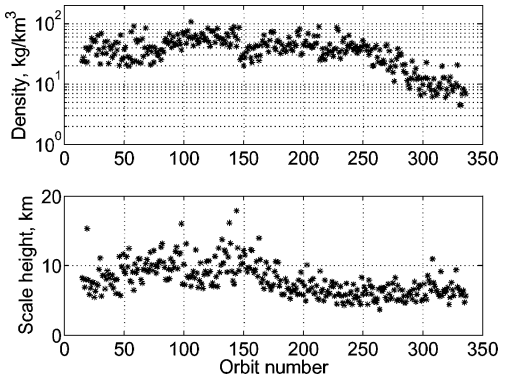

Fig. 12 Periapsis density and density scale height.

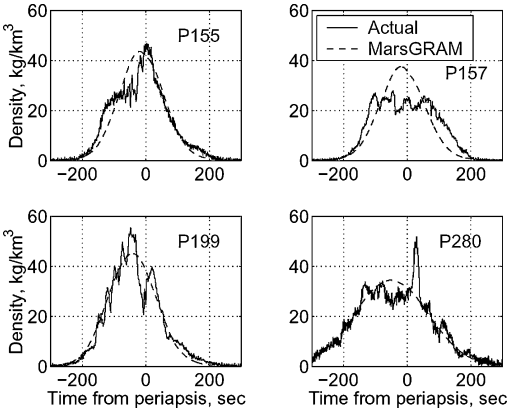

Fig. 13 Other atmospheric density profiles.

inbound and outbound at 140 km, whereas only a factor of 2.5 was measured. From an overall mission viewpoint, this would be considered a typical comparison.

Figure 12 shows the periapsis density and density scale height for each orbit during aerobraking. These results are derived by performing a least-squares fit to the log density profile using all of the data within 10 km of the periapsis altitude to determine $\rho(h_0)$ and H_s in Eq. (3). The periapsis density variation shows the main aerobraking phase up to about orbit 250, where solar array temperature is the controlling factor. The main phase is followed by the walk-out phase, where orbit lifetime is the major consideration. Note from Fig. 3 that periapsis altitude is smoothly decreasing up to orbit 100, yet the periapsis density only slightly reflects this trend, and up to orbit 75 the orbit-to-orbit variations can be up to a factor of four. Orbits 100–150 are at about the same altitude, and the orbit-to-orbit variability is much smaller than the earlier orbits or later orbits. During this time, periapsis is above 80°N latitude, and the lack of variability is interpreted as being inside the polar vortex, which is discussed later in detail.

During the first 100 orbits, density scale height (temperature) increases as periapsis precesses toward the pole and altitude decreases (Fig. 3). This is an unexpected result because both trends were expected to result in a decrease in temperature. The anomalistic trend has been interpreted[15] as a winter polar mesospheric warming that raised the entire temperature structure of the upper atmosphere in the polar region. Such a phenomena was not predicted by the MarsGRAM model and may not be an annual event.

Other Density Profiles

As was experienced during MGS, there are a number of interesting phenomena that have occurred in the exploration of the thermosphere of Mars using aerobraking. Examples of these are shown in Fig. 13. The equivalent MarsGRAM profile is also plotted for comparison. The outbound leg of orbit 155 shows a traditional bell-shaped variation with time closely following MarsGRAM. Periapsis occurs at about 82°N latitude and 270°E longitude. The outbound leg is poleward of periapsis. The bump in the inbound leg at −100 s

is about twice the equivalent outbound density and occurs at about 75° latitude. These types of profiles were interpreted as crossing the polar vortex. There are highly variable wavelike structures outside and near the vortex and relatively smooth variations inside the vortex. The polar vortex is similar to the northern hemisphere jet stream on Earth that is highly variable in both time and space, but that generally rotates with the planet while migrating eastward. Orbit 157 has nearly the same ground track as orbit 155, but with periapsis at 162°E longitude. The interpretation here is that periapsis is outside the vortex in this longitude range. Latitudinal waves are increasing the density variations at both −100 and +75 s and decreasing it near periapsis, resulting in the plateau shown.

By orbit 199, periapsis has precessed to 72°N. The inbound leg has five waves up to maximum density. For these waves, the peak to trough density ratios vary between 1.2 and 1.9, and the peaks are about 2° apart in latitude. The last peak, just after periapsis, is followed by a very low variability outbound leg after 75 s at a latitude of 78°. The interpretation is that the vortex boundary is near 76°, giving a highly variable profile up to 75 s while outside the vortex and low variability inside the vortex after 75 s. Finally, orbit 280 is included to show that local phenomena can produce nearly factor of two changes in density over very short timescales. The latitude range goes from 25°N at −200 s to 63°N at +200 s. The spike just after periapsis has a latitude width of about 2°. The Mars thermosphere is noted for the large spatial and temporal variability. As with MGS,[3] small spatial scale variations of this order occur on a majority of passes. On at least one MGS pass,[13] there is a compelling argument that density changed by a factor of five in less than 5 s, during which the spacecraft traveled about 1.3 km lower in altitude and 20 km downtrack. For an aerobraking mission, note that the solar array temperature is the limiting factor and that conduction through the solar array smooths many of these short-term variations, thus, such local peaks may contribute little to the maximum temperature.[6]

Using Accelerometer Data for Prediction

Given the variability discussed earlier, several different methods were used to predict density for future orbits. Essentially all of the methods were used each day and evaluated and compared.

Persistence and MarsGRAM Scaling

The simplest prediction method is persistence, that is, the assumption that the density profile for the next orbit will be the same as the last orbit. Because the altitudes may be different, periapsis density from the last orbit $\rho(n)$ is mapped to the periapsis altitude $h(n+1)$ of the next orbit via the density scale height $H_s(n)$, using Eq. (3) to yield the estimate

$$\hat{\rho}(n+1) = \rho(n) \exp \frac{-[h(n+1) - h(n)]}{Hs(n)} \tag{4}$$

When the density and scale heights in Fig. 12 and the altitudes from Fig. 3 are used, the ratios of actual for the next orbit to the predicted for the next orbit are as shown in Fig. 14. The mean ratio is 1.10, and the standard deviation over the entire phase is 0.49. The biased estimate is due to the overweighing of a large ratio compared to the reciprocal of a large ratio. The orbit-to-orbit variability is clearly larger during the first and last 75 orbits. The early high variability is associated with waves near the polar vortex. After periapsis has precessed into the polar region and moved into the nighttime (Fig. 3), variability decreases. As periapsis precesses toward the equatorial region, near the end of aerobraking, variability again increases. However, as will be seen, this increase is due more to the lower signal-to-noise ratios associated with walk-out than it is due to waves.

MGS aerobraking took below 60°N, so that the polar vortex was not encountered, but MGS did show orbit-to-orbit variability of about 40% 1-σ, and a substantial fraction of this variability was due to stationary waves in the middle-latitude region.[4] Explanation of such waves[16] suggests that the stationary property is an artifact of sampling from a nearly inertially fixed orbit. The underlying waves are actually moving in the Mars atmosphere. Nevertheless, a large

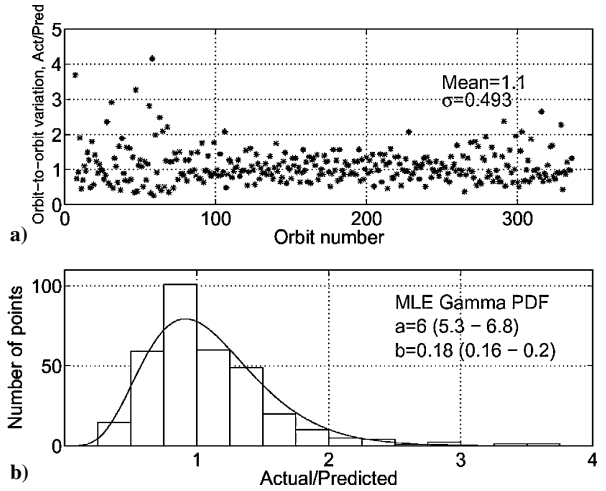

Fig. 14 Prediction capability for persistence throughout aerobraking.

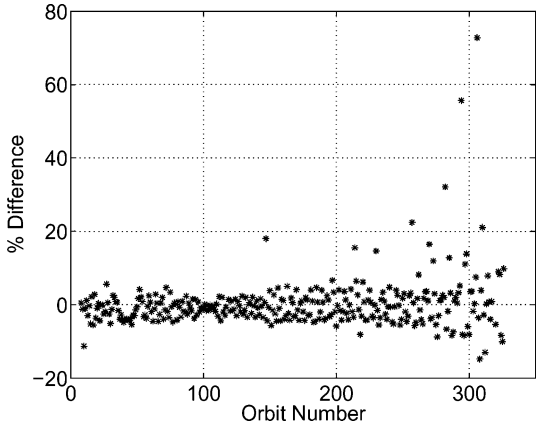

Fig. 15 Comparison of total drag ΔV from radio tracking and accelerometer data.

fraction of the orbit-to-orbit variability was modeled as stationary waves during MGS operations.[3] MGS persistence was found to follow a gamma probability distribution function.[4] Figure 14b provides the maximum likelihood estimate of the gamma distribution that fits Odyssey persistence. The parameters a and b are such that $a \times b$ is the mean, and b is the variance of the sample. With each estimate is shown the 95% confidence interval. For MGS,[4] $a = 7.4$ (6.7–9.2) and $b = 0.14$ (0.13–0.16). The Mars atmospheric model proposed for Odyssey Monte Carlo simulations[4] gave gamma distribution parameters of $a = 6.9$ (6.1–7.6) and $b = 0.16$ (0.14–0.17) and provided an intermediate distribution that overlaps the distributions of the two missions. Thus, even though the underlying physical process for the large variability seems to be different for the two missions, the statistical distribution of orbit-to-orbit variability is very similar.

Another simple approach is to scale the MarsGRAM density profile to have the same area under the curve as the accelerometer-derived density profile. This essentially means that the scaled MarsGRAM profile would have provided the same effective ΔV as was measured by the accelerometers. Except for the small differences in drag coefficient models, this scaling provides a direct comparison with the NAV calculated ΔV and an independent check on both approaches. Figure 15 provides a comparison of these two methods in the form of the percent difference of the accelerometer derived ΔV and the NAV radio tracking ΔV divided by the accelerometer value. Over the entire mission, the mean difference is 0.12% with an rms difference of 7%. The large deviations during walk-out are due to the total ΔV becoming small, and so the signal-to-noise ratio for both methods is increasing. Although the drag is high and periapsis is inside the vortex, the agreement is within the uncertainty produced by the utilization of two C_y models as discussed earlier.

Stationary and Moving Waves

During MGS aerobraking, longitudinal density waves were detected.[3] As mentioned earlier, the current explanation is that these waves are eastward moving on Mars that propagate around the planet in about 1 sol (one Martian day: 24 h 39 min). Consequently, they appear to be fixed in longitude because the observations are taken in an orbit with slow nodal precession. Before this insight was available, the waves were modeled as stationary waves relative to the rotating planet for MGS operations. The waves are identified with wave numbers, for example, wave 1 goes through a complete sine cycle in 360° of longitude, and wave 2 goes through a complete cycle in 180°. Waves 1–5 were detected at various times during the MGS mission[13] and were used as a basis[4] for preflight simulations using MarsGRAM.[14]

Based on the MGS experience, such stationary waves were expected for Odyssey, and AMT procedures called for development of wave models on a daily basis. Unlike MGS, these models generally proved to have little predictive capability. It was soon found that assuming that the waves moved in longitude provided improved prediction, but again this capability was not sustained for extended periods of time. The wave modeling, therefore, proved to be of limited quantitative value during operations, but it did provide qualitative knowledge on the state of the atmosphere that aided in making some maneuver decisions.

Postflight analysis of the data provided insight into the wave structure. The amplitude and phase of wave 1 are shown in Fig. 16. These results are based on daily least-squares solutions for the mean density and only stationary wave 1 amplitude and phase. At least 12 orbits or 3 days of data, whichever is greater, are included in each solution. Up to day 32, there are 12 orbits in each solution, and after that there are 3 days of data. The first solution encompasses 7 days, and the last solution includes 36 orbits. Amplitude is given as a fraction of the mean density. In each solution set, the periapsis density (Fig. 12) is mapped, using the periapsis scale height, to the highest altitude in the set. Amplitude increases up through day 18 as periapsis approaches the pole, with the peak amplitude of 70% occurring when periapsis latitude is about 77°. Periapsis is north of 80° from day 25 to day 43, and the amplitude is significantly lower, which might be considered as being inside the vortex. Periapsis is at 75° and precessing south on day 47. Passing through the vortex during this time only produces an amplitude of 25%. Outside the high-latitude region the amplitude averages about 20%.

It is clear that wave 1 is generally progressing eastward throughout the entire aerobraking phase at an average rate of about 17°/day. MGS results for northern latitudes less than 60° had average amplitudes of about 15%, but the phase remained relatively constant.[4]

Results from a similar analysis for wave 2 are given in Fig. 17. Like wave 1, peak amplitude occurs before entering the vortex and decreases thereafter. Wave 2 also drifts eastward until the vortex

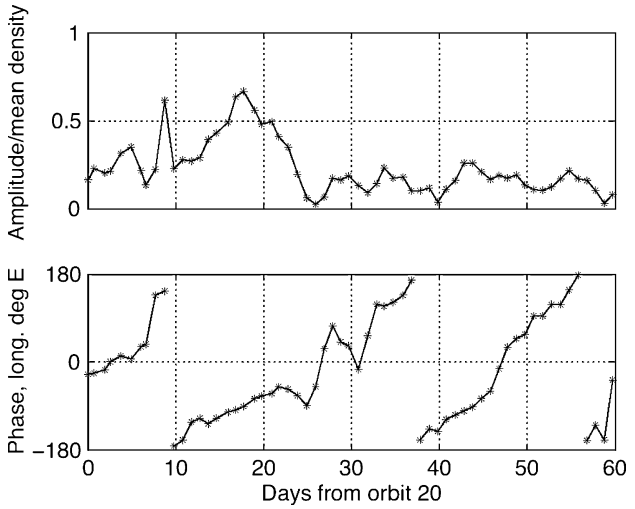

Fig. 16 Wave 1 amplitude and phase based on 12 orbits or three-day fit to near periapsis density.

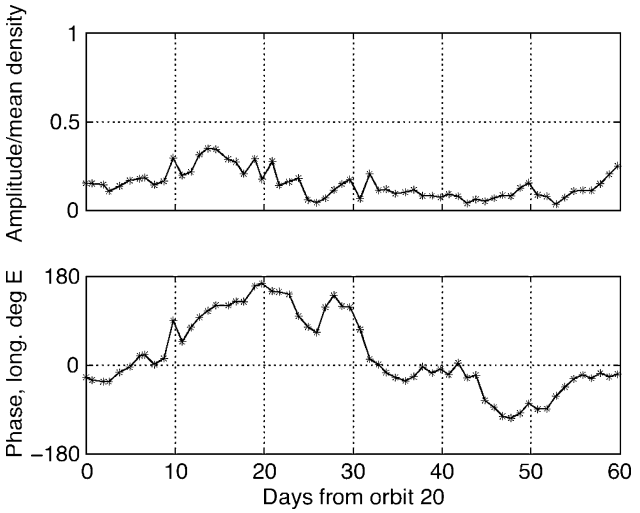

Fig. 17 Wave 2 amplitude and phase based on 12 orbits or three-day fit to near periapsis density.

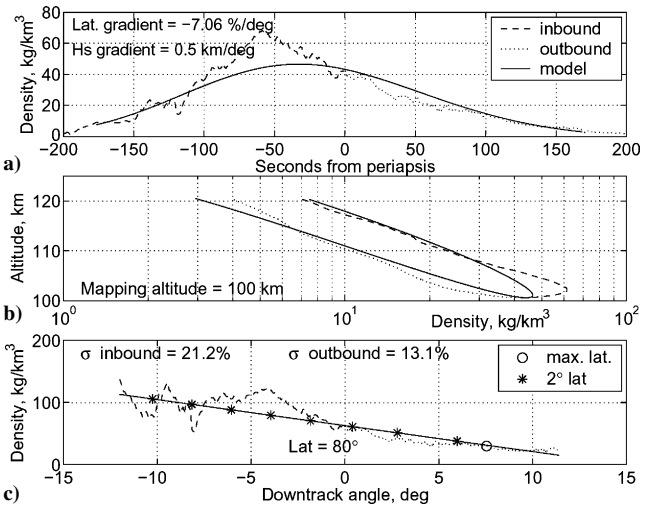

Fig. 18 Example of mapping to a reference altitude for wave detection, P159.

is encountered, then drifts westward until out of the vortex. The amplitude of about 10% for the last 15 days is consistent with MGS amplitudes in the 30–60° latitude range. However, during MGS, the phase was relatively constant at about 50°E. Thus, even though there are some similarities with MGS, there are differences perhaps due to season, dust storm, or local solar time differences.

Mapping to Reference Altitude and Polar Plots

Encountering the polar vortex required developing new analysis methods as the need arose. The persistent large waves that were seen on the inbound legs of the initial orbits suggested an increased risk as periapsis precessed toward the pole. It was of interest to quantify these waves in terms of the equivalent periapsis density variations. A number of approaches were attempted, but the best approach was to map the entire density profile to periapsis or some other altitude using a simple model of the atmosphere. The model used Eq. (3) and assumed that both the density and scale height at the reference altitude vary linearly with latitude or downtrack angle. Downtrack angle or true anomaly was used when periapsis was near the pole and latitude was not monotone over the pass. This approach presents a nonlinear optimization problem that was solved using an off-the-shelf constrained optimization routine. Convergence was robust, but on occasions the solution was constrained by the upper and lower bounds.

A typical result is shown in Fig. 18. Figure 18a shows the 7-s mean density profile and the model fit to these data. The maximum densities differ significantly. The density latitudinal gradient is about

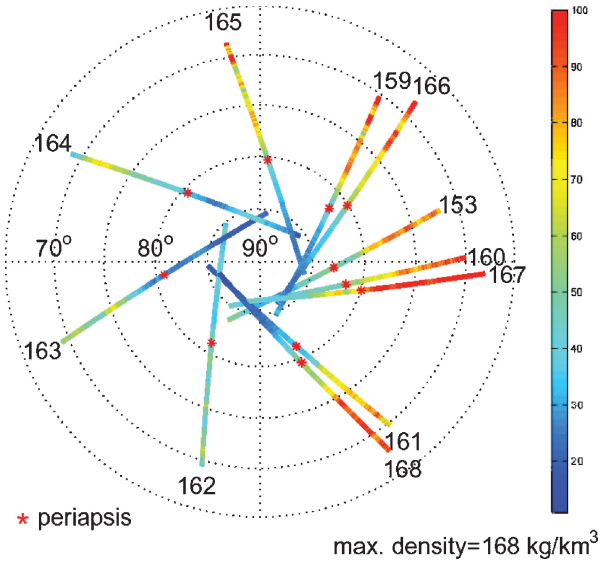

Fig. 19 Polar plot of densities mapped to 100-km altitude for orbits 153 and 159–168, density truncated at 100 kg/km^3 to enhance variability.

7%/° downtrack, and the scale height gradient is at the upper limit constraint of 0.5 km/° downtrack. The scale height constraint corresponds to about 7% change in temperature per degree. Figure 18b gives the altitudinal variation using the 39-point average density. Note that the density changes by a factor of three within 3 km of periapsis, suggesting very strong latitudinal gradients or wave activity. Figure 18c shows both the model and measured densities mapped to an altitude of 100 km using the model. The track is closest to the pole at about 7° outbound. The dots correspond to 2° latitude increments with periapsis occurring at about 82°. Apsidal regression is moving periapsis to the left Fig. 18c, and so one interpretation is that approximately 4° ahead there is a region where the density is about twice as great at the same periapsis altitude. Also, the rms deviation from the model is 21.2% of the model density inbound and only 13.1% outbound, again demonstrating that inside the vortex the variability is much less than outside the vortex. Like the terrestrial northern hemisphere jet stream, features such as those shown in Fig. 18 are known to be highly variable in both space and time.

In an attempt to understand the temporal and spatial variations, polar plots of the density variation were made daily for orbits from the previous days. One such polar plot is shown in Fig. 19. Each track in Fig. 19 shows the density along the orbit path on a latitude–longitude polar plot. All of the measured densities have been mapped to a common reference altitude, in this case 100 km. Each mapping is done using results similar to those in Fig. 18. The densities correspond to the data line in the lower subplot. The maximum predicted density of 168 kg/km^3 corresponds to the beginning of the inbound track for orbit 167. To accentuate the along track variations, the gray scale is truncated at 100 kg/km^3. Periapsis is identified by an asterisk on each track. The time between close orbit pairs, for example, 160 and 167, is about 1 sol, and such adjacent pairs were compared to generate confidence in the mapping and to identify trends in the movement of the density field. A strong wave 1 pattern is clearly evident at this time, with maximum density occurring in the first and fourth quadrants. Furthermore, along-track variability is small within 10° of the pole and increases as latitude moves south. Along-track variability is most apparent in orbits 159, 165, and 166. The strong latitudinal density gradient away from the polar region is also quite evident, particularly in the first and fourth quadrants. Plots such as these in Fig. 19 were generated daily and provided considerable insight into the density morphology.

Conclusions

Aerobraking at Mars is both an opportunity and a challenge. Even if accurate predictive models were available, spacecraft design, mission design, and operations would have to account for about a factor of two change in density from orbit to orbit or else be prepared to make periapsis trim maneuvers nearly every orbit. Accelerometer data complements radio tracking data in providing another means of obtaining the ΔV due to drag on each pass. Furthermore, these data provide information on the physical processes behind the variability, can be used to quantify the spatial and temporal variations, and will lead to improved Martian thermospheric models and understanding.

Acknowledgments

This work was sponsored by the NASA Mars 2001 Odyssey project office and NASA Langley Research Center.

References

[1]Lyons, D. T., "Aerobraking Magellan: Plan versus Reality," *Advances in the Astronautical Sciences*, Vol. 87, Pt. 2, 1994, pp. 663–680.

[2]Lyons, D. T., Beerer, J. G., Esposito, P., and Johnston, M. D., "Mars Global Surveyor: Aerobraking Mission Overview," *Journal of Spacecraft and Rockets*, Vol. 36, No. 3, 1999, pp. 307–313.

[3]Tolson, R. H., Keating, G. M., Cancro, G. J., Parker, J. S., Noll, S. N., and Wilkerson, B. L., "Application of Accelerometer Data to Mars Global Surveyor Aerobraking Operations," *Journal of Spacecraft and Rockets*, Vol. 36, No. 3, 1999, pp. 323–329.

[4]Dwyer, A. M., Tolson, R. H., Munk, M. M., and Tartabini, P. V., "Development of a Monte Carlo Mars-GRAM Model for Mars 2001 Aerobraking Simulations," *Journal of the Astronautical Sciences*, Vol. 50, No. 2, 2002, pp. 191–211.

[5]Tartabini, P. V., Munk, M. M., and Powell, R.W., "Development and Evaluation of an Operational Aerobraking Strategy for Mars Odyssey," *Journal of Spacecraft and Rockets*, Vol. 42, No. 3, 2005, pp. 423–434.

[6]Dec, J. A., Gasbarre, J. F., and George, B. E., "Thermal Analysis and Correlation of the Mars Odyssey Spacecraft's Solar Arrays During Aerobraking Operations," AIAA Paper 2002-4536, Aug. 2002.

[7]Smith, J. C., Jr., and Bell, J. L., "2001 Mars Odyssey Aerobraking," *Journal of Spacecraft and Rockets*, Vol. 42, No. 3, 2005, pp. 406–415.

[8]Takashima, N., and Wilmoth, R.G., "Aerodynamics of Mars Odyssey," AIAA Paper 2002-4809, Aug. 2002.

[9]Hanna Prince, J. L., Chavis, Z. Q., and Wilmoth, R. G., "Modeling Reaction-Control-System Effects on Mars Odyssey," *Journal of Spacecraft and Rockets*, Vol. 42, No. 3, 2005, pp. 444–449.

[10]Cestaro, F. J., and Tolson, R. H., "Magellan Aerodynamic Characteristics During the Termination Experiment Including Thruster Plume–Free Stream Interactions," NASA CR-1988-206940, March 1998.

[11]Antreasian, P. G., Baird, D. T., Border, J. S., Burkhard, P. D., Graat, E. J., Jah, M. K., Mase, R. A., McElrath, T. P., and Portock, B. M., "2001 Mars Odyssey Orbit Determination During Interplanetary Cruise," *Journal of Spacecraft and Rockets*, Vol. 42, No. 3, 2005, pp. 394–405.

[12]Mase, R. A., Antreasian, P. G., Bell, J. L., Martin-Mur, T. J., and Smith, J. C., Jr., "Mars Odyssey Navigation Experience," *Journal of Spacecraft and Rockets*, Vol. 42, No. 3, 2005, pp. 386–393.

[13]Tolson, R. H., Keating, G. M., Noll, S. N., Baird, D. T., and Shellenberg, T. J., "Utilization of Mars Global Surveyor Accelerometer Data for Atmospheric Modeling," *Astrodynamics 1999*, Vol. 103, American Astrodynamics Society, San Diego, CA, 1999, pp. 1329–1346.

[14]Justus, C. G., and James, B. F., "Mars Global Reference Atmospheric Model 2000 Version (Mars-GRAM 2000) Users Guide," NASA TM-2000-21-279, May 2000.

[15]Keating, G. M., Tolson, R. H., Theriot, M. E., Jr., Hanna, J. L., Dwyer, A. M., Bougher, S. W., and Zurek, R. W., "Detection of Winter Polar Warming in Mars Upper Atmosphere," Proceedings of the European Geophysical Society 27th General Assembly, Symposium PS1.02: Terrestrial Planets: Atmospheres. Nice-Acropolis Congress Center, April 2002.

[16]Wilson, J., and Hamilton, K., "Comprehensive Model Simulation of Thermal Tides in the Martian Atmosphere," *Journal of Atmospheric Sciences*, Vol. 53, May 1996, pp. 1290–1326.

R. Mase
Guest Editor